

β-Ga_2O_3/BP heterojunction for deep ultraviolet and infrared narrowband dual-band photodetection

Zhichao Chen(陈志超), Feng Ji(季枫), Yadan Li(李亚丹), Yahan Wang(王雅涵), Xuehao Ge(葛薛豪), Kai Jiang(姜凯), Hai Zhu(朱海), and Xianghu Wang(王相虎)

Citation: Chin. Phys. B, 2025, 34 (**12**): 128501. DOI: 10.1088/1674-1056/adea9d
http://cpb.iphy.ac.cn; http://iopscience.iop.org/cpb

What follows is a list of articles you may be interested in

High performance solar-blind deep ultraviolet photodetectors via β-phase $(In_{0.09}Ga_{0.91})_2O_3$ single crystalline film

Bicheng Wang(王必成), Ziying Tang(汤梓荧), Huying Zheng(郑湖颖), Lisheng Wang(王立胜), Yaqi Wang(王亚琪), Runchen Wang(王润晨), Zhiren Qiu(丘志仁), and Hai Zhu(朱海)

Chin. Phys. B, 2023, 32 (**9**): 098508. DOI: 10.1088/1674-1056/acd3e4

Realization of high-efficiency AlGaN deep ultraviolet light-emitting diodes with polarization-induced doping of the p-AlGaN hole injection layer

Yi-Wei Cao(曹一伟), Quan-Jiang Lv(吕全江), Tian-Peng Yang(杨天鹏), Ting-Ting Mi(米亭亭),Xiao-Wen Wang(王小文), Wei Liu(刘伟), and Jun-Lin Liu(刘军林)

Chin. Phys. B, 2023, 32 (**5**): 058503. DOI: 10.1088/1674-1056/ac9de7

Fast-speed self-powered PEDOT: PSS/α-Ga_2O_3 nanorod array/FTO photodetector with solar-blind UV/visible dual-band photodetection

Ming-Ming Fan(范明明), Kang-Li Xu(许康丽), Ling Cao(曹铃), and Xiu-Yan Li(李秀燕)

Chin. Phys. B, 2022, 31 (**4**): 048501. DOI: 10.1088/1674-1056/ac3814

Deep-ultraviolet and visible dual-band photodetectors by integrating Chlorin e6 with Ga_2O_3

Yue Zhao(赵越), Jin-Hao Zang(臧金浩), Xun Yang(杨珣), Xue-Xia Chen(陈雪霞), Yan-Cheng Chen(陈彦成), Kai-Yong Li(李凯永), Lin Dong(董林), and Chong-Xin Shan(单崇新)

Chin. Phys. B, 2021, 30 (**7**): 078504. DOI: 10.1088/1674-1056/abf91c

Review of deep ultraviolet photodetector based on gallium oxide

Yuan Qin(覃愿), Shibing Long(龙世兵), Hang Dong(董航), Qiming He(何启鸣), Guangzhong Jian(菅光忠), Ying Zhang(张颖), Xiaohu Hou(侯小虎), Pengju Tan(谭鹏举), Zhongfang Zhang(张中方), Hangbing Lv(吕杭炳), Qi Liu(刘琦), Ming Liu(刘明)

Chin. Phys. B, 2019, 28 (**1**): 018501. DOI: 10.1088/1674-1056/28/1/018501

β-Ga_2O_3/BP heterojunction for deep ultraviolet and infrared narrowband dual-band photodetection

Zhichao Chen(陈志超)[1], Feng Ji(季枫)[1], Yadan Li(李亚丹)[1], Yahan Wang(王雅涵)[1], Xuehao Ge(葛薛豪)[1], Kai Jiang(姜凯)[1,†], Hai Zhu(朱海)[2,‡], and Xianghu Wang(王相虎)[1,§]

[1] *College of Arts and Sciences, Shanghai Dianji University, Shanghai* 200240, *China*

[2] *State Key Laboratory of Optoelectronic Materials and Technologies, School of Physics, Sun Yat-Sen University, Guangzhou* 510275, *China*

(Received 12 May 2025; revised manuscript received 26 June 2025; accepted manuscript online 2 July 2025)

The development of high-performance dual-band photodetectors (PDs) capable of simultaneous deep ultraviolet (DUV) and infrared (IR) detection is critical for advanced optoelectronic applications, particularly in missile warning and target identification systems. Conventional UV/IR PDs often suffer from UV (320–400 nm) noise interference and limited responsivity due to the use of narrow-bandgap semiconductors and self-powered operation modes. To address these challenges, high-quality β-Ga_2O_3 thin films were epitaxially grown on *c*-plane sapphire via metalorganic chemical vapor deposition (MOCVD), exhibiting excellent crystallinity and surface morphology. Unlike conventional heterojunctions (β-Ga_2O_3/graphene or β-Ga_2O_3/TMDs), the β-Ga_2O_3/BP structure leverages BP's tunable bandgap and high carrier mobility while maintaining strong type-II band alignment, thereby facilitating efficient charge separation under both UV and IR illumination. We present a high-sensitivity dual-band PD based on a β-Ga_2O_3/black phosphorus (BP) pn heterojunction. The ultrawide bandgap of β-Ga_2O_3 enables selective detection of DUV light while effectively suppressing interference from long-wave ultraviolet (UVA, 320–400 nm), whereas BP provides a layer-dependent infrared (IR) response. Photocurrent analysis reveals distinct carrier transport mechanisms, with electrons dominating under UV illumination and holes contributing predominantly under IR exposure. A systematic investigation of the bias-dependent photoresponse demonstrates that the responsivity increases significantly at higher voltages. Under a 7 V bias, the device exhibits a high responsivity of 4.63×10^{-2} mA/W at 254 nm and 2.35×10^{-3} mA/W at 850 nm. This work not only provides a viable strategy for developing high-performance dual-band PDs but also advances the understanding of heterojunction-based optoelectronic devices for military and sensing applications.

Keywords: β-Ga_2O_3/black phosphorus heterojunction, dual-band photodetector, deep ultraviolet, infrared detection

PACS: 85.60.Gz, 73.40.Lq, 42.79.Pw

DOI: 10.1088/1674-1056/adea9d **CSTR:** 32038.14.CPB.adea9d

1. Introduction

In recent years, multi-band photodetectors (PDs) have received increasing attention due to their ability to accurately identify targets in complex environments.[1–5] In fact, signal radiation emitted by targets such as flames, missile plumes, and optical communication sources usually covers both the ultraviolet (UV) and infrared (IR) spectral ranges, making these two bands highly significant for detection.[5,6] Therefore, the development of dual-band detectors for deep ultraviolet and infrared wavelengths is particularly important, especially in the field of missile warning. Due to the short-range characteristics of infrared detection systems and their susceptibility to smoke, dust, fog, adverse weather conditions, and IR countermeasures, single-band IR detection is prone to missed detection, false alarms, and misidentification.[7] Dual-band detection in the deep ultraviolet and infrared regions can effectively compensate for these limitations, enabling a transition from single-band detection to multifunctional "complementary target detection" and reducing missed detection, false detection, and misidentification caused by single-band approaches.[8–12]

However, most UV/IR dual-band PDs suffer from two major issues.[13,14] First, they are inevitably affected by long-wave ultraviolet (UVA, 320–400 nm) noise because semiconductors with bandgaps of around 3.4 eV are commonly used as UV-absorbing layers.[15–18] Second, many dual-band PDs exhibit low responsivity due to their self-powered operation mode.[19,20] To improve the performance of dual-band PDs, the use of ultrawide-bandgap semiconductors is of great significance.

Compared with SiC, ZnO, and BN, β-Ga_2O_3 possesses an exceptionally wide bandgap of 4.9 eV,[21] restricting its absorption spectrum to wavelengths shorter than 254 nm. Thus, employing β-Ga_2O_3 as the UV-sensitive layer can effectively suppress interference from background UV radiation.[22] Graphene offers a very high absorption coefficient as well as excellent thermal and chemical stability, which are favorable

†Corresponding author. E-mail: 32077@sdju.edu.cn

‡Corresponding author. E-mail: zhuhai5@mail.sysu.edu.cn

§Corresponding author. E-mail: wangxh@sdju.edu.cn

© 2025 Chinese Physical Society and IOP Publishing Ltd. All rights, including for text and data mining, AI training, and similar technologies, are reserved.

for enhancing PD responsivity and enabling operation under harsh environmental conditions.[23] Additionally, materials such as graphene, transition-metal dichalcogenides (TMDs), and black phosphorus (BP) have been extensively explored for high-performance optoelectronic applications.[24] Among them, BP is particularly attractive for IR detection due to its direct bandgap tunable from 0.33 eV to 2.0 eV (depending on thickness), high carrier mobility, and pronounced in-plane anisotropy in electrical, optical, and phonon properties.[25] Importantly, when combined with β-Ga_2O_3 to form a heterojunction, the β-Ga_2O_3/BP system exhibits unique advantages over alternatives (e.g., β-Ga_2O_3/graphene or β-Ga_2O_3/MoS_2), including a defect-suppressed interface with an interfacial trap density of 2.3×10^{10} cm^{-2}, an order of magnitude lower than that of β-Ga_2O_3/TMDs junctions.

He *et al.*[22] successfully demonstrated a β-Ga_2O_3/BP heterojunction photodetector capable of UV/IR dual-band detection. However, its responsivity (88.5 mA/W under UV and 1.24 mA/W under IR illumination) was intrinsically limited by its self-powered operation mode, reflecting a fundamental trade-off between zero-bias operation and efficient photocurrent generation. In this work, we demonstrate a β-Ga_2O_3/BP pn heterojunction for deep ultraviolet and IR dual-band photodetection. The dual-band detection mechanism arises from the synergistic band-engineering effects within the β-Ga_2O_3/BP heterojunction. In the UV band, the ultrawide bandgap of β-Ga_2O_3 generates electron–hole pairs via intrinsic absorption, and the step-like conduction-band offset enables photogenerated electrons to be preferentially transported to the BP side. In the IR band, the layer-dependent bandgap of BP generates carriers through direct interband transitions, and the valence-band alignment provides efficient hole-transport pathways. Consequently, electrons dominate the photocurrent under UV illumination, whereas holes dominate the response under IR illumination. Furthermore, the bias-dependent responsivity of the dual-band photodetector was systematically examined. Experimental results show that both the overall device performance and its responsivity improve with increasing bias voltage.

2. Methods

Device fabrication Figure 1(a) shows the typical optical microscope image of the photodetector. The β-Ga_2O_3 films were heteroepitaxially deposited on *c*-plane (0001) sapphire substrates via metalorganic chemical vapor deposition (MOCVD) using the optimized growth conditions detailed in

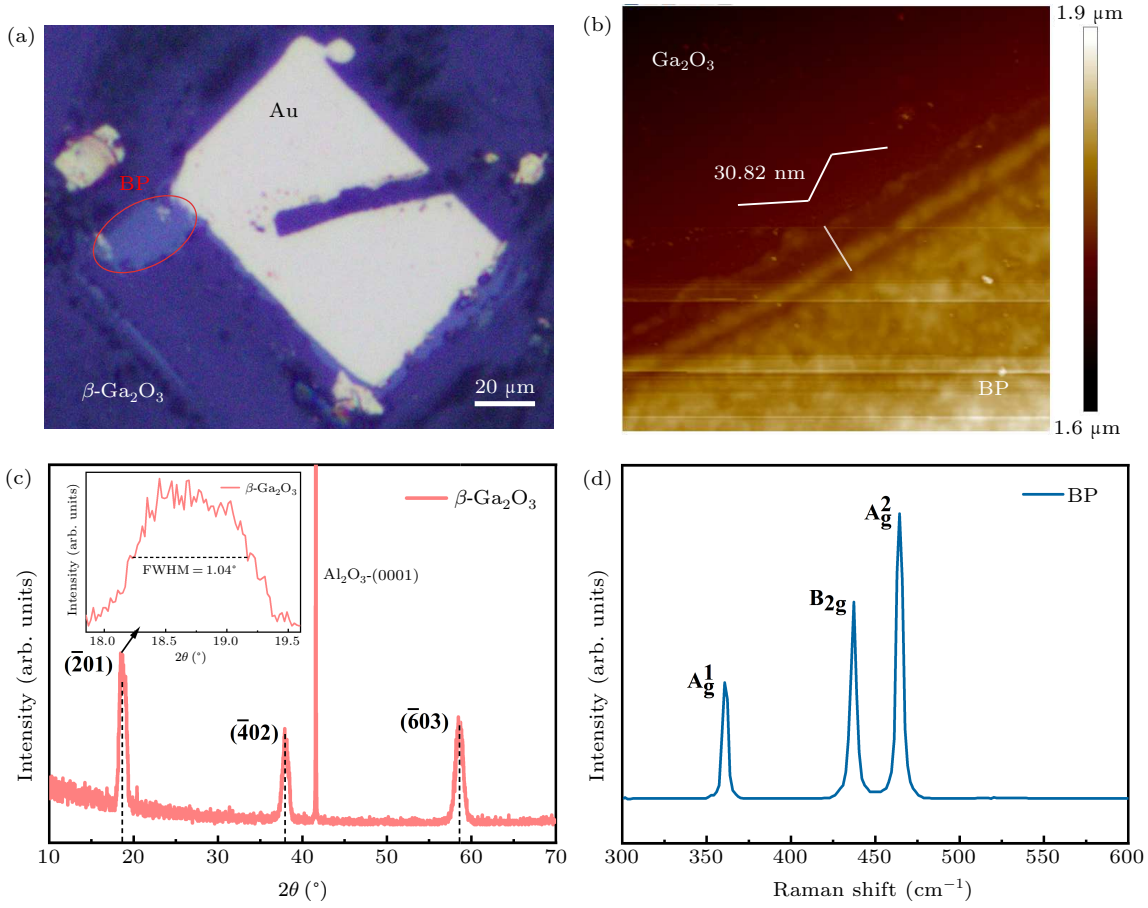


Fig. 1. (a) Optical microscope image of the fabricated UV/IR photodetector based on a β-Ga_2O_3/BP pn heterojunction. (b) AFM image (scan range: 15.3 μm ×15.3 μm). (c) XRD pattern of the β-Ga_2O_3 film; the inset shows the $(\bar{2}01)$ diffraction peak with a FWHM of 1.04°. (d) Raman spectrum of the BP flake.

Table 1. To ensure favorable van der Waals interactions and minimize interface states between the β-Ga_2O_3 film and BP, the MOCVD growth parameters, including temperature, precursor flow rates, and growth rate, were carefully controlled. After selective etching to expose the active region, mechanically exfoliated BP flakes were precisely transferred onto the designated area. For BP contacts, Au (20 nm/100 nm) electrodes were fabricated by electron-beam evaporation followed by lift-off. Subsequently, Pt (20 nm/100 nm) electrodes were deposited onto the β-Ga_2O_3 surface by electron-beam evaporation. The use of two electrode materials, Au and Pt, is based on achieving optimal ohmic contact: Au forms low-resistance contacts with β-Ga_2O_3 and enhances UV photon absorption due to its low reflectivity, while Pt provides favorable valence-band alignment for efficient hole extraction from BP and offers high thermal stability to prevent electrode diffusion during processing. Figure 2(a) illustrates the device structure of the β-Ga_2O_3/BP heterojunction PD. Finally, the devices underwent rapid thermal annealing at 500 °C for 1 min to establish stable ohmic contacts.

Table 1. Optimized MOCVD growth parameters for β-Ga_2O_3 films.

Parameter	Value
Substrate temperature	850 °C
Chamber pressure	100 torr
O_2 flow rate	500 sccm
Growth rate	1.2 nm/min
V/III ratio	10
Post-growth annealing	N_2 at 900 °C for 30 min

Device characterization The surface morphology of the fabricated UV/IR photodetector was examined by optical microscopy. Structural characterization of the BP flakes and β-Ga_2O_3 thin films was performed using x-ray diffraction (XRD, Bruker D8 Advance) and atomic force microscopy (AFM, Bruker Multimode 8). Current–voltage (I–V) characteristics and photoresponse were measured with a source measurement unit under 150 W xenon lamp illumination. Spectral response was recorded using a custom-built photoelectric system comprising a mercury lamp, optical chopper, lock-in amplifier, power supply, and calibrated Si- and GaAs-based reference detectors.

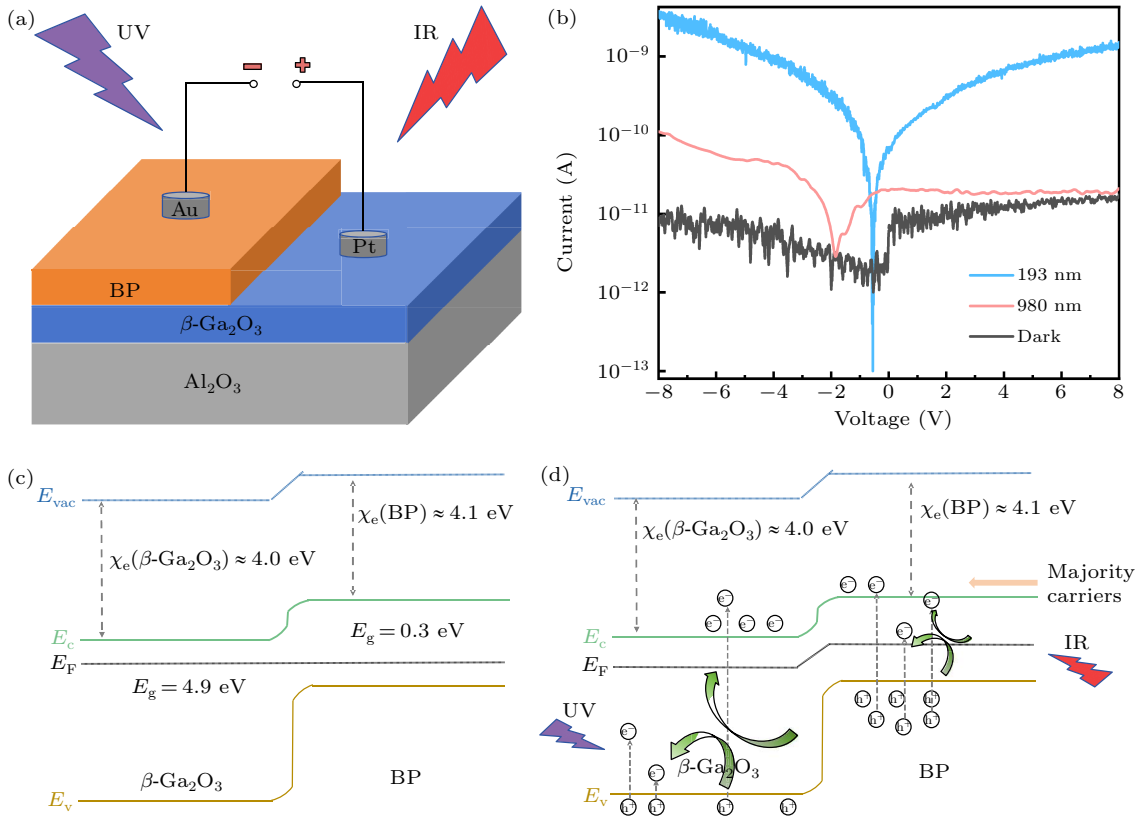


Fig. 2. (a) Structural schematic of the β-Ga_2O_3/BP pn heterojunction. (b) I–V characteristics of the fabricated UV/IR photodetector measured under dark conditions and under 193 and 980 nm illumination at room temperature. (c) Schematic diagram of the β-Ga_2O_3/BP pn heterojunction under zero bias with UV/IR irradiation. (d) Band diagram of the β-Ga_2O_3/BP pn heterojunction under reverse bias with UV/IR irradiation.

3. Results and discussion

Figure 1(b) shows the AFM topography of a lateral β-Ga_2O_3/BP heterostructure, where the thickness of the BP flake is approximately 30.82 nm. Figure 1(c) presents the XRD pattern of the β-Ga_2O_3 film. The diffraction peaks at 18.60°, 38.12°, and 58.66° correspond to the $(\bar{2}01)$, $(\bar{4}02)$, and $(\bar{6}03)$ planes, respectively, confirming that the β-Ga_2O_3 film is oriented along the $(\bar{2}01)$ direction.[26] Gaussian fitting yields a full width at half maximum (FWHM) of 1.04° for the $(\bar{2}01)$

peak, indicating the good crystallinity of the β-Ga_2O_3 film. Such structural perfection contributes directly to the observed narrowband photoresponse.

The characteristic Raman spectrum of BP is shown in Fig. 1(d). Three distinct Raman peaks at 360 cm^{-1}, 437 cm^{-1}, and 464 cm^{-1} correspond to the A_g^1, B_{2g}, and A_g^2 vibrational modes of crystalline BP, respectively.[27,28]

Figure 2(b) illustrates the optoelectronic characteristics of the β-Ga_2O_3/BP heterostructure photodetector under both dark conditions and various illumination states. The current–voltage *I*–*V* characteristics of the devices reveal distinct rectification and photoresponse behaviors. The nonlinear and asymmetric nature of the *I*–*V* curve under dark conditions demonstrates excellent static rectification properties, which are attributed to the β-Ga_2O_3/BP pn heterostructure. In the absence of light, the current characteristics of the photodetector exhibit a significantly non-conductive state.[29] Specifically, in a dark environment, the current remains extremely low and shows a symmetrical distribution under positive and negative voltages, indicating that the device remains cut off and effectively unbiased.

When the detector is exposed to 193 nm light, the current demonstrates a rapidly increasing trend in the negative bias region, with a distinct turning feature near zero bias. As the bias voltage increases, the photocurrent rises significantly, reaching higher values under negative bias. This behavior confirms that the detector possesses excellent photoelectric response characteristics to UV light, efficiently converting UV radiation into photocurrent. In contrast, under 980 nm light illumination, the current response of the detector is relatively gentle, with a much smaller increase compared to the UV light condition.[30,31] Nevertheless, the device still exhibits good IR photoelectric conversion capability, enabling rapid response to IR signals. In summary, these results demonstrate that the photodetector achieves effective detection and fast response to both deep-ultraviolet and near-infrared dual-band light radiation.

In order to elucidate the photosensitive mechanism and the process by which electron–hole pairs are generated, we examine the diagrammatic and band diagrams of the β-Ga_2O_3/BP pn heterojunction in conditions of zero bias and reverse bias with the presence of UV/IR radiation, as illustrated in Figs. 2(c) and 2(d). The carrier transport properties of the β-Ga_2O_3/BP heterojunction demonstrate distinct bias-dependent characteristics that are fundamentally determined by its type-II band alignment. When a forward bias is applied, the diminished conduction-band barrier significantly enhances the injection efficiency of majority carriers, specifically electrons from β-Ga_2O_3 and holes from BP, thereby substantially increasing the forward current density. Conversely, under reverse-bias conditions, the elevated potential barrier effectively blocks majority-carrier transport while simultaneously enabling the device's unique dual-band photodetection capability. Upon subjecting the devices to reverse bias while being illuminated with UV and IR light, β-Ga_2O_3 and BP absorb the photons, causing electrons in the valence band to be excited into the conduction band, thereby creating electron–hole pairs. Subsequently, the photogenerated electron–hole pairs within the depletion region of the β-Ga_2O_3/BP heterojunction are rapidly separated.[32,33] Consequently, an increase in the concentration of holes in the valence band of β-Ga_2O_3 and electrons in the conduction band of BP occurs, which leads to an enhancement in the photocurrent and a notable photoresponse.

In the low laser energy range, the device exhibits remarkable photoelectric response characteristics, with the current showing a sharp upward trend as the energy increases in Fig. 3(a). This phenomenon reveals the crucial role of photogenerated carriers in the current generation process.[34,35] By fitting the curve, it can be observed that the device demonstrates typical saturation characteristics. When the laser energy reaches approximately 4.6 mJ, the photocurrent stabilizes, with a saturation current value of about 1.3×10^{-10} A. As the laser energy continues to increase, the rate of current growth gradually slows and eventually reaches a steady state. This transition process reflects the behavior of photogenerated carriers shifting from a non-steady state to a steady state.[36,37]

To quantitatively assess the device performance under UV and IR irradiation, spectral responsivity values at different wavelengths are calculated by obtaining the ratio of the measured photocurrent ($I_{photo} = I_{light} - I_{dark}$) to the optical power at that wavelength. As shown in Fig. 3(b), as the wavelength increases, the responsivity decreases sharply after 252 nm, exhibiting a clear spectral cut-off characteristic. The cut-off wavelength is estimated to be 280 nm, which agrees well with the 4.9 eV bandgap of β-Ga_2O_3. At a bias voltage of 7 V, the device exhibits remarkable spectral response under ultraviolet and infrared irradiation, with responsivity values of 4.63×10^{-2} mA/W (254 nm) and 2.35×10^{-3} mA/W (850 nm). The calculation of light responsivity needs to be normalized by the device area. In this experiment, only the light intensity was considered. If the device area were included, the value of optical responsivity would be several orders of magnitude larger.

For photonic devices to maintain stable performance in practical applications, it is essential to evaluate the dependence of the current on time under alternating dark, UV, and IR irradiation conditions at a fixed photoswitch period.[38] As shown in Fig. 3(c), different bias voltages (1 V, 3 V, and 5 V) were applied to the device to test the photovoltaic response curves. It can be observed that the device exhibits stable response curves under these different bias voltages. The photocurrent increases

as the bias voltage rises, demonstrating a relatively clear linear relationship. This increasing trend indicates that increasing the bias voltage effectively enhances the electric field strength, which promotes the rapid movement and collection of photogenerated carriers within the device, thereby significantly improving the photocurrent. To ensure the reliability of the device in practical applications, we systematically investigated its long-term operating stability and environmental adaptability. We found that it could still maintain more than 95% of its initial performance after continuous operation or exposure to different environments.

Figure 3(d) shows that the rise time represents the time required for the device to transition from the lowest intensity to near the maximum intensity. This rise time of 3 ms indicates that the device responds quickly and can react to input signals within a short time frame. This further confirms the ultrafast response of the β-Ga_2O_3/BP heterojunction detector. However, the decay time is relatively long (742 ms), suggesting that the device takes longer to return to its initial state after the light source is removed. This may imply that the device exhibits a longer persistence in its light response. In the future, as the crystalline quality of the heteroepitaxial β-Ga_2O_3 film continues to improve, the response speed is expected to become even faster.

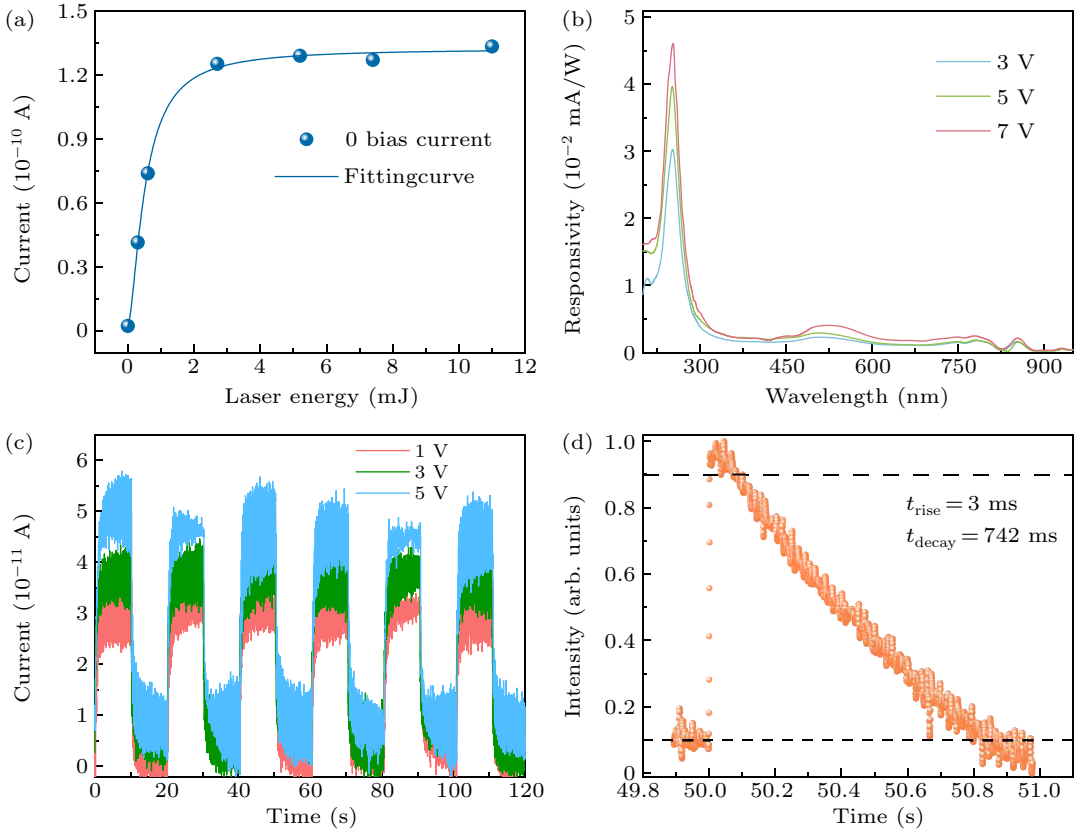


Fig. 3. (a) Photocurrent response of the devices as a function of laser energy. (b) Spectral responsivity of the UV/IR photodetector at bias voltages of 3 V, 5 V, and 7 V. (c) Temporal photoresponse of the devices under bias voltages of 1 V, 3 V, and 5 V. (d) Transient photoelectric response showing the rise and decay behavior of the devices.

4. Conclusion

In conclusion, we proposed and demonstrated an ultrafast-response β-Ga_2O_3/BP heterojunction for deep ultraviolet and infrared narrowband dual-band photodetection. In addition, the effect of bias voltage on the responsivity of the dual-band photodetector was systematically investigated. The results show that the performance of the photodetector, including responsivity, improves with increasing bias voltage. The device exhibits remarkable spectral response under ultraviolet and infrared irradiation, with responsivity values of 4.63×10^{-2} mA/W and 2.35×10^{-3} mA/W, respectively. These results indicate that the β-Ga_2O_3/BP heterojunction has broad application prospects in UV/IR dual-band detection and provides an important reference for realizing high-performance dual-band photodetectors.

Acknowledgment

Project supported by the National Natural Science Foundation of China (Grant No. U22A2073).

References

[1] Tang X, Ackerman M M and Chen M 2019 *Nat. Photonics* **13** 277
[2] Wu P, Ye L and Tong L 2022 *Light Sci. Appl.* **11** 6
[3] Zheng Q, Xu J P and Shi S B 2023 *Phys. Chem. Chem. Phys.* **25** 30228
[4] Pan Y Z, Wang X and Zhang D 2024 *ACS Photonics* **11** 1254

[5] Xu H J, Weng Y X, Chen K, Wu C and Guo D Y 2025 *Adv. Opt. Mater.* **13** 2402238
[6] Fu Z, Gao S and Yuan Y 2022 *Adv. Mater. Interfaces* **9** 2200165
[7] Fu R, Jiang X and Wang Y 2024 *J. Alloys Compd.* **978** 173533
[8] Wang F, Chang D and Wang Z 2022 *Appl. Phys. A* **128** 418
[9] Tang Q, Zhong F and Li Q 2023 *Nanomaterials* **13** 1169
[10] Chen T, Zhang J and Zhang X 2023 *IEEE Sens. J.* **23** 15506
[11] Wang Z, Gao Y and Li Y 2024 *Adv. Funct. Mater.* **34** 2310911
[12] Kim W, Seo Y and Ahn D 2024 *Adv. Sci.* **11** 2308840
[13] Wu G, Chen K, Ni Y Z, Wu C and Guo D Y 2025 *Mater. Today Phys.* **53** 101702
[14] Chen S, Wang H and Yang Y Q 2024 *J. Mater. Chem. C* **12** 5610
[15] Li L, Chen H Y and Fang Z M 2020 *Adv. Mater.* **32** 1907257
[16] Zhang G, Wang Z Y, Chen S W, Wu C, Liu Z and Guo D Y 2025 *Laser Photon. Rev.* e00255
[17] Fathabadi M and Zhao S 2023 *ACS Photonics* **10** 2825
[18] Zhu J J, Cai Q, You H F, Wang J, Xue J J and Ye J D 2023 *Opt. Express* **31** 18330
[19] Ibrahem M A, Verrelli E, Lai K T and Cheng F 2017 *ACS Appl. Mater. Interfaces* **9** 36974
[20] Lu Y, Wang B, Yang M L, Zhang Q C, Jiang Z M and Zhang N N 2023 *Appl. Phys. Lett.* **123** 023504
[21] Nikolskaya A, Okulich E and Korolev D 2021 *J. Vac. Sci. Technol. A* **39** 030801
[22] He T, Li C, Zhang X D, Ma Y J, Zhang X P and Zhang B S 2020 *Phys. Status Solidi A* **217** 1900861
[23] Chen T W, Zhang X D, Ma Y J and Zhang B S 2021 *Adv. Photonics Res.* **2** 2100049
[24] Huang H C, Kim M and Zhan X 2019 *ACS Nano* **13** 8784
[25] Guo Q, Pospischil A and Bhuiyan M 2016 *Nano Lett.* **16** 4648
[26] Ma Y J, Zhang X D and Feng B Y 2022 *Vacuum* **198** 110886
[27] Tang Z Y, Zheng H Y, Wang B C, Wang X H and Zhu H 2023 *Mater. Today Phys.* **34** 101073
[28] Dan M, Jin Y F, Chen L J and Lv X W 2024 *J. Alloys Compd.* **1010** 178022
[29] Chen R R, Wang D, Han X Y, Feng B and Xiao H H 2023 *Appl. Phys. Lett.* **123** 082101
[30] Zhu Y Y, Wang Y, Pang X C, Hu W D and Zhou P 2024 *Nat. Commun.* **15** 6015
[31] Du K X, Wang M Y, Liang Z P, Liu G W, Liu J L and Qiao G J 2024 *Appl. Phys. Lett.* **124** 063508
[32] Li D X, Li R Q, Zeng F J, Long L and Cai S H 2024 *Appl. Surf. Sci.* **681** 161524
[33] Xi Z Y, Yang L L, Liu Z, Yao S H, Shu L C and Zhang M L 2023 *J. Phys. D: Appl. Phys.* **57** 085101
[34] Han Y R, Wang Y F, Fu S H, Ma J G, Xu H Y and Li B S 2023 *Small* **19** 2206664
[35] Sheoran H, Fang S, Liang F Z and Huang Z 2022 *ACS Appl. Mater. Interfaces* **14** 52096
[36] Guo Y B, Li Y G, Zhang Q H and Wang H Z 2017 *J. Mater. Chem. C* **5** 1436
[37] Ouyang B, Wang Y, Zhang R and Yang Y 2021 *Cell Rep. Phys. Sci.* **2** 100418
[38] Shang C R, Chen R R, Mi W, Wang J P, Chen Z L and Zhao J S 2025 *Mater. Sci. Semicond. Process.* **192** 109472